Goal-Oriented Adaptivity using Unconventional Error Representations for 1D Helmholtz Equation ☆

Vincent Darrigrand[a,b], David Pardo[a,c,d], Ignacio Muga[e]

[a] *University of the Basque country, Leioa, Spain*
[b] *Project-Team INRIA Magique-3D, INRIA Bordeaux-Sud Ouest, France.*
[c] *Basque center for applied Mathematics, Bilbao, Spain.*
[d] *Ikerbasque, Bilbao, Spain.*
[e] *Pontificia Universidad Católica de ValparaÃso, Chile.*

Abstract

In this work, the error of a given output functional is represented using bilinear forms that are different from those given by the adjoint problem. These representations can be employed to design novel h, p, and hp energy-norm and goal-oriented adaptive algorithms. Numerical results in 1D show that, for wave propagation problems, the advantages of this new representation are notorious when selecting the Laplace equation as the dual problem. Specifically, the upper bounds of the new error representation are sharper than the classical ones used in both energy-norm and goal-oriented adaptive methods, especially when the dispersion (pollution) error is significant.

Keywords: Goal oriented adaptivity, Finite element methods, Error representation, Helmholtz equation

1. Introduction

In finite element methods (FEM), adaptivity plays a fundamental role in order to obtain accurate solutions using limited computational resources. While adaptive algorithms were first designed to accurately approximate the energy norm of a problem [5, 4], many engineering applications require a good approximation of a specific quantity of interest. An energy norm driven self-adaptive

☆The first two authors were partially funded by the Project of the Spanish Ministry of Economy and Competitiveness with reference MTM2013-40824-P, the CYTED 2011 project 712RT0449, and the Basque Government Consolidated Research Group Grant IT649-13 on "Mathematical Modeling, Simulation, and Industrial Applications (M2SI)". The second author was also partially funded by the BCAM "Severo Ochoa" accreditation of excellence SEV-2013-0323. The last author was partially funded by the CYTED 2011 project 712RT0449 and the FONDECYT project 1130776.

Email addresses: vincent.darrigrand@gmail.com (Vincent Darrigrand), dzubiaur@gmail.com (David Pardo), ignacio.muga@gmail.com (Ignacio Muga)

Published on March 2015 http://dx.doi.org/10.1016/j.camwa.2015.03.006

strategy can still be used for that purpose, although it often becomes sub-optimal and unable to provide an accurate solution for the required quantity of interest in a reasonable amount of time.

For example, in [30, 32] authors deal with a problem in which electromagnetic fields are measured at a receiver antenna in a lossy media. In that situation, the amplitude of the measurement is several orders of magnitude smaller at the receiver than at the source, because of the energy dissipation through the medium. Thus, a small relative error of the solution in the energy-norm may not imply a small relative error at the receiver. The classical energy norm adaptive approach may procure relative errors of the quantity of interest surpassing 15%, whereas the global energy norm error is below 0.01%, see Figure 1.

[Figure 1 about here.]

During the late 90's, an approach to overcome this issue appeared: the so-called goal-oriented strategy. The goal-oriented approach consists in expressing the error in the quantity of interest as an integral over the entire computational domain involving the errors of the original and adjoint problems, and then minimise an upper bound of such error representation by performing local refinements. For symmetric problems, the energy-norm approach becomes a particular case of the goal-oriented one that corresponds to the situation in which the quantity of interest and the load vector of the original problem coincide, as it occurs in several waveguide problems [13, 35].

The goal-oriented procedure has been actively developed and applied in the last two decades. Some of the most prominent works in the area include those developed by Rannacher et al. [8, 9, 39], who use the terminology of *weighted a posteriori error control* ; Peraire, Patera et al. [29, 28, 36, 24, 37, 41] who employed the term *output functional* when studying upper and lower a posteriori estimates of the error in the quantity of interest; and J.T. Oden & S. Prudhomme [38, 25], who introduced the term *goal oriented adaptivity* in this context. We can find applications in structural problems and visco-elasticity [27, 48, 22, 21], in fluid-structure interactions [46, 45, 47], and in control theory [15, 17, 16]. The goal oriented adaptivity is also a key feature for some inverse problems, like the determination of the composition of the underground. In [34, 32, 33], the authors applied the goal oriented adaptivity to a logging-while-drilling problem. A multi-goal oriented approach developed in [31] was applied to magnetotelluric problems in [1]. In summary, the study of goal oriented adaptivity is essential for multiple engineering applications.

Using the adjoint problem, most authors represent the approximation error in the quantity of interest via the global bilinear form that describes the problem in terms of local and computable quantities. Then, different strategies are devised to obtain sharp upper bounds of such error representation. For example, in [38], authors introduce a scalar parameter intended to improve the sharpness of the bound. In [26], the author introduces dual estimators of the functional error that are based on dual residual weighting and on dual error estimate weighting. These estimators result to be asymptotically exact with respect to the error in the quantity of interest.

Our methodology, however, is based on the selection of an alternative bilinear form exhibiting better properties than the original bilinear form (e.g. positive definiteness). We represent the residual error functional of the adjoint problem through this alternative form. We can then compute new upper bounds of the error of the quantity of interest in a similar way to the classical approach. The main contribution of this paper is to demonstrate that a proper choice of such alternative form may improve the upper bounds of the error representation. Moreover, the method proposed here generalises the existing ones, since, in particular, we can select as the alternative bilinear form the one associated to the adjoint problem.

In this paper, we describe the method for general 1D, 2D, and 3D problems, but we illustrate it numerically with a 1D-Helmholtz example. We select the Helmholtz equation for several reasons: this equation is widely used in applications having a transmitter-receiver structure where goal oriented strategies are needed, the weak Helmholtz bilinear form is not positive definite, and the discrete solution is known to be numerically unstable for high wavenumbers because of dispersion errors and pollution effects [19, 18, 2, 3, 20, 6]. As we shall demonstrate throughout the paper, the advantages of the proposed method are clear from the simplest 1D problem. Our upper bounds are sharper than the classical ones if one selects wisely the alternative operator.

Extensive numerical results are illustrated using uniform h- and p-refinements, as well as a simple self-adaptive goal-oriented p-refinement strategy. The application to other adaptive algorithms such as a goal-oriented hp-adaptive algorithm [32, 35], adaptivity in a high continuity space [7, 11, 23], or adaptivity in time domain [10] is straightforward.

The rest of the paper is organised as follows: in section 2, we present the details of our new methodology compared to the classical approach. In section 3, we describe the model problem that will be used to illustrate our method: the 1D Helmholtz equation. In section 4, we present the adaptive algorithms used to produce the numerical results. Section 5 is devoted to numerical results and illustrations of the advantages and limitations of the proposed method. The main conclusions are stated in section 6.

2. Method

We start this section with some definitions and notation. Let $\Omega \subset \mathbb{R}^N$ be an open domain and $\mathbb{H} := \mathbb{H}(\Omega)$ a Hilbert space on Ω. Let Ω_h be a disjoint partitioning of Ω into open elements K such that $\overline{\Omega} = \cup_{K\in\Omega_h} \overline{K}$. For each $K \in \Omega_h$, we consider the space $\mathbb{H}_K$ containing the restrictions to K of functions of $\mathbb{H}$. A continuous bilinear form $a : \mathbb{H} \times \mathbb{H} \to \mathbb{R}$ is said to be *localisable* if

$$a(u, v) = \sum_{K\in\Omega_h} a_K(u, v), \qquad \forall u \in \mathbb{H}, \forall v \in \mathbb{H},$$

where a_K denotes the *restriction* of a to the space $\mathbb{H}_K \times \mathbb{H}_K$. If a is also symmetric and positive definite, then it defines a norm on $\mathbb{H}$ and semi-norms

on each $\mathbb{H}_K$. We denote them by

$$\|\cdot\|_a := \sqrt{a(\cdot,\cdot)} \quad \text{and} \quad |\cdot|_{a_K} := \sqrt{a_K(\cdot,\cdot)},$$

respectively.

2.1. Variational problem

We set b to be a localisable symmetric continuous bilinear form and f a continuous linear form, both defined on $\mathbb{H}$. Let $\mathbb{V}_h \subset \mathbb{H}$ be a finite dimensional Galerkin approximation space of $\mathbb{H}$, related to the partitioning Ω_h. Let us consider the following variational formulation and its discrete equivalent:

Find $u^* \in \mathbb{H}$, $u_h^* \in \mathbb{V}_h$ such that

$$b(u^*, v) = f(v), \qquad \forall v \in \mathbb{H}, \tag{2.1}$$
$$b(u_h^*, v_h) = f(v_h), \qquad \forall v_h \in \mathbb{V}_h. \tag{2.2}$$

We assume that the solutions of these variational formulations are unique. Thus, we can define the error function as $e_h := u^* - u_h^*$.

For goal-oriented approaches, we provide an output functional l that defines the quantity of interest for which we want to obtain a small relative error. For example, an output functional can be the average of a function (or a derivative) over a small subset $\Omega_S \subset \Omega$, i.e.,

$$l(u) = \frac{1}{|\Omega_S|}\int_{\Omega_S} u\, dx \quad \text{or} \quad l(u) = \frac{1}{|\Omega_S|}\int_{\Omega_S} \nabla u \cdot \vec{\alpha}\, dx, \quad \text{for some } \vec{\alpha} \in \mathbb{R}^N.$$

We assume that l is a linear and continuous form on $\mathbb{H}$. The goal of computations from the engineering point of view is to *sharply* estimate $|l(u)|$. For that purpose, the main idea of goal-oriented adaptivity is to control the error $|l(e_h)|$. This is achieved by finding a sharp upper bound that is expressed in terms of computable norms that are guaranteed to decrease as one performs grid refinements.

2.2. Error representations

2.2.1. Classical approach

The core of the goal oriented approach is to use the adjoint problems of (2.1) and (2.2) respectively:

Find $v^* \in \mathbb{H}$ and $v_h^* \in \mathbb{V}_h$ such that

$$b(u, v^*) = l(u), \qquad \forall u \in \mathbb{H}, \tag{2.3}$$
$$b(u_h, v_h^*) = l(u_h), \qquad \forall u_h \in \mathbb{V}_h. \tag{2.4}$$

We assume that problems (2.3) and (2.4) are well-posed so the dual error function $\varepsilon_h := v^* - v_h^*$ is well defined. Let $\hat{b}$ be a localisable symmetric positive definite bilinear form on $\mathbb{H}$ such that:

$$|b_K(u,v)| \leqslant |u|_{\hat{b}_K} |v|_{\hat{b}_K}. \tag{2.5}$$

We use $\hat{b}$ since the b form may not be positive definite and therefore we cannot define a norm or semi-norm from it. For instance, if b is the weak form of the Helmholtz operator $(-\Delta - k^2)(\cdot)$, then $\hat{b}$ may be selected as the weak form of the operator $(-\Delta + k^2)(\cdot)$.

By plugging solutions u^* and u_h^* into (2.3) and (2.4) respectively, and using the *localisable* property of b, we obtain the following local estimation:

$$|l(e_h)| = |b(e_h, v^*)| \leqslant \sum_{K \in \Omega_h} |b_K(e_h, v^*)| \leqslant \sum_{K \in \Omega_h} |e_h|_{\hat{b}_K} |v^*|_{\hat{b}_K}.$$

We observe that v^* is independent of the discretisation and does not decrease with mesh refinements. However, the error e_h of the direct problem is b-orthogonal to $\mathbb{V}_h$. In particular $b(e_h, v^*) = b(e_h, \varepsilon_h)$. Therefore, we can improve the upper bound of $|l(e_h)|$ by introducing a quantity that decreases faster with the mesh refinements:

$$|l(e_h)| = |b(e_h, \varepsilon_h)| \leqslant \sum_{K \in \Omega_h} |b_K(e_h, \varepsilon_h)| \leqslant \sum_{K \in \Omega_h} |e_h|_{\hat{b}_K} |\varepsilon_h|_{\hat{b}_K}. \tag{2.6}$$

For details, see [38].

2.2.2. New approach

The objective of our new approach is to improve the upper bound of the error in the quantity of interest $|l(e_h)|$ by obtaining sharper upper bounds.

Let $\widetilde{b}$ be an arbitrary localisable symmetric, elliptic and continuous bilinear form. We define our elliptic representation of the dual residual error functional, as the solution of the problem:

> Find $\widetilde{\varepsilon}_h \in \mathbb{H}$ such that:
>
> $$\widetilde{b}(u, \widetilde{\varepsilon}_h) = l(u) - b(u, v_h^*), \quad \forall u \in \mathbb{H}. \tag{2.7}$$

By the Lax-Milgram theorem (or Riesz representation), the variational formulation (2.7) has a unique solution on $\mathbb{H}$. A similar idea called *elliptic error representation* was introduced by A. Romkes & J.T. Oden [40] in the context of modelling error analysis for adaptive modelling.

Observe that $\widetilde{\varepsilon}_h$ must decrease with mesh refinements since it represents an error functional that depends continuously on the error ε_h. Moreover, $\widetilde{\varepsilon}_h$ is $\widetilde{b}$-orthogonal to $\mathbb{V}_h$:

$$\widetilde{b}(u_h, \widetilde{\varepsilon}_h) = l(u_h) - b(u_h, v_h^*) = 0, \quad \text{for all } u_h \in \mathbb{V}_h.$$

But the powerful idea behind introducing (2.7), is that we can represent the error in the quantity of interest as:

$$l(e_h) = b(e_h, \varepsilon_h) = l(e_h) - b(e_h, v_h^*) = \widetilde{b}(e_h, \widetilde{\varepsilon}_h).$$

Hence, we get the new estimate:

$$|l(e_h)| = \left|\widetilde{b}(e_h, \widetilde{\varepsilon}_h)\right| \leqslant \sum_{K\in\Omega_h} \left|\widetilde{b}_K(e_h, \widetilde{\varepsilon}_h)\right| \leqslant \sum_{K\in\Omega_h} |e_h|_{\widetilde{b}_K} |\widetilde{\varepsilon}_h|_{\widetilde{b}_K}, \tag{2.8}$$

If problem (2.7) is well-posed but the $\widetilde{b}$ form is non-elliptic, then only the last inequality in (2.8) is not true. In that case we make use of an inequality such as (2.5). That is the reason why this method generalises the existing ones.

In this paper, we show numerically that there often exists a $\widetilde{b}$ so that estimate (2.8) is sharper than estimate (2.6). Additionally, the proposed method to represent the error given by equation (2.8) intrinsically provides a great flexibility that allows us to apply it to a wide range of 1D, 2D and 3D problems.

3. Model problem

Given $k \in \mathbb{R}$, let us consider the following problem:

Find $u^* \in H^1(0,1)$ such that,

$$\begin{cases} -\left(\dfrac{d^2}{dx^2} + k^2\right) u^* = 1 & \text{on } (0,1), \\ u^*(0) = 0, \dfrac{du^*}{dx}(1) = -\dfrac{1}{2}. \end{cases} \tag{3.1}$$

We set $\mathbb{H} \coloneqq \{v \in H^1(0,1), v(0) = 0\}$. Then

$$b(u,v) = \int_0^1 \left(\frac{du}{dx}\frac{dv}{dx} - k^2 uv\right) dx, \qquad f(v) = \int_0^1 v\, dx - \frac{v(1)}{2}.$$

For illustrative purposes, we define the following linear output functional:

$$l(u) = \int_{2/5}^{4/5} u\, dx. \tag{3.2}$$

We set the 1D-Laplace bilinear form as the alternative form $\widetilde{b}$, that is:

$$\widetilde{b}(u,v) = \int_0^1 \frac{du}{dx}\frac{dv}{dx} dx, \quad \forall u, v \in \mathbb{H}.$$

There exist several ways to compute numerically the errors. One is to use the analytical solution and the approximated solution on V_h. In our case, we know the analytical solution of the direct problem (3.1):

$$u^*(x) = \mathfrak{R}e\left(Ae^{ikx} + Be^{-ikx} - \frac{1}{k^2}\right),$$

where

$$A = \frac{2k - 2e^{ki}i + k^2 e^{ki} i}{2k^3 \left(e^{2ki} + 1\right)} \qquad \text{and} \qquad B = -\frac{e^{ki}\left(k^2 - 2 + 2ke^{ki}i\right) i}{2k^3 \left(e^{2ki} + 1\right)}.$$

However, we do not know the exact solution of the adjoint problem (2.3) nor the solution of our new problem (2.7). Thus, we work with two approximation spaces: "coarse" and "fine". The coarse one is given by any finite element discretisation, while the fine space is obtained from the coarse one by performing some global refinement in such a way that most of the coarse grid error is reproduced by the difference between the fine and coarse grid solutions. In our case, we build the fine grid by increasing uniformly the polynomial order of approximation by two for the p-adaptive algorithm.

4. Refinement algorithms

This section describes the mesh refinement algorithms considered here, namely a h-uniform refinement algorithm and a goal-oriented p-adaptive strategy. The p-uniform refinement algorithm is a particular case of the p-adaptive strategy and its details have been omitted.

4.1. Uniform h-refinements

We compute the solutions and errors using Algorithm 1. From these errors, we can evaluate and compare upper bounds (2.6) and (2.8). For Algorithm 1, we set the following parameters: the number of elements of the discretisation N and the uniform polynomial order of approximation p. We set the wavenumber k such that for a given N and p, the minimum number of degrees of freedom per wavelength is small (less than 3). Then, we select a set of structured meshes until we reach a number of degrees of freedom per wavelength close to 100. We consider one additional finer mesh as our reference mesh for error estimation. Then, we solve the direct (2.2) and adjoint (2.4) Helmholtz problems on every mesh. From there, we can compute the errors e_h and ε_h and, by solving the new dual problem given by (2.7), the quantity $\widetilde{\varepsilon}_h$.

[Algorithm 1 about here.]

4.2. Goal-oriented p-adaptive algorithm.

Algorithm 2 describes our $1D$ self-adaptive p-refinement strategy.

[Algorithm 2 about here.]

The algorithm follows the classical adaptive pattern described in Figure 2.

[Figure 2 about here.]

We work with two meshes: "coarse" and "fine". The fine mesh is defined from the coarse one by increasing the polynomial order by two on each element. We assume that the fine mesh error is significantly smaller than the coarse one, so that the fine mesh solution can be used as a reference solution. We compute then the approximate and reference solutions of the direct (2.2) and adjoint (2.4) problems, as well as the corresponding approximate errors e_h and ε_h. Subsequently, we solve the new dual problem (2.7) in order to compute $\widetilde{\varepsilon}_h$. Next, we estimate the relative error on the quantity of interest using (2.8). If the error tolerance is not satisfied (otherwise, the algorithm is terminated), we select for refinement those elements with a local error indicator close to the maximum one. Then, refinements are performed by increasing the polynomial order of approximation by one on the selected elements. The resulting grid is the starting 'coarse' grid for the next iteration.

To ensure the convergence of the algorithm, we compute the errors by projecting the reference solution on the coarse mesh (cf. [42] for details).

5. Numerical Results

In this section, we compare the upper bounds of the error representation given by the classical and the proposed methods:

$$|l(e_h)| \text{ (error in the quantity of interest)},$$

$$\sum_{K\in\Omega_h} |b_K(e_h,\varepsilon_h)| \text{ (Classical bound)}, \tag{5.1}$$

$$\sum_{K\in\Omega_h} \left|\widetilde{b}_K(e_h,\widetilde{\varepsilon}_h)\right| \text{ (New bound)}. \tag{5.2}$$

From the mathematical standpoint, using the above upper bounds is controversial. First, because in the "Classical bound" (5.1), the bilinear form of model problem (3.1) is indefinite and one cannot ensure that uniform grid refinements will monotonically reduce that bound, unless the grid is assumed to be sufficiently small with respect to the wavenumber, so the problem at the element level becomes positive semi-definite. Even in this last situation, the associated cosine of the angle between e_h and ε_h can still behave erratically under mesh refinements. A similar problem can be experimented with bound (5.2), since the cosine of the angle between e_h and $\widetilde{\varepsilon}_h$ cannot be controlled under mesh refinements.

Stable upper bounds can be easily derived, as shown in (2.6) and (2.8). However, practitioners often employ error bound (5.1) (despite the fact that it is mathematically unstable), since it is sharper than (2.6) and frequently provides better results [34]. In here, we follow this practical approach, and we compare (5.1) vs (5.2). We have also compared results utilising the mathematically stable upper bounds given by (2.6) and (2.8). However, we have omitted these results in the paper, since they are qualitatively similar to those observed with the practical approach, and provide no further insights.

5.1. Uniform p-refinements

First, we consider the case $l \equiv f$. In this case the direct and adjoint problems coincide, so do their errors $e_h = \varepsilon_h$ and $\widetilde{e}_h = \widetilde{\varepsilon}_h$. Notice that this is the choice corresponding to classical energy-norm adaptive algorithms [13, 14].

Figure 3 shows numerically that the new bound provides a sharper estimation of the error in the quantity of interest $l(e_h)$ when performing uniform p-refinements. We also distinguish two different phases: (a) the pre-asymptotic phase, where the new upper bound is much sharper than the classical one, and (b) the asymptotic phase where both bounds coincide.

[Figure 3 about here.]

We now represent the L^2-norm and H^1-semi-norm of the errors e_h and $\widetilde{e}_h$. That last quantity is obtained by solving the problem:

> Find $\widetilde{e}_h \in \mathbb{H}$ such that:
>
> $$\widetilde{b}(\widetilde{e}_h, v) = b(e_h, v) \quad \forall v \in \mathbb{H}.$$

Figure 4 shows that the norms of the error in the tilde-version are smaller than the regular ones in the pre-asymptotic phase and approach each other in the asymptotic regime. The idea behind that the tilde-version of any error is smaller seems to be that the new approach softens (or eliminates) the pollution effect of the Helmholtz equation. The pollution effect of the Helmholtz equation is discussed in [6, 43, 44] for instance. This observation may explain why we obtain sharper estimates using $\widetilde{e}_h$. The second interesting fact is that $\|\nabla e_h\|_{L^2(0,1)}$ and $k\,\|e_h\|_{L^2(0,1)}$ are of the same order for the pre-asymptotic phase. This does not occur for the tilde-versions.

[Figure 4 about here.]

5.1.1. Pollution error elimination

As we previously mentioned, one reason for observing better results with the new bounds seems to be the reduction of the pollution error. This idea is further confirmed by the numerical results presented in Figure 5, showing that for few degrees of freedom per wavelength (in the pre-asymptotic range, Sub-figures [5(a),5(b),5(c)]), $\widetilde{e}_h$ is less affected than e_h by the pollution effect that arises when increasing the wavenumber k. When we consider a larger number of degrees of freedom per wavelength so that we are studying the asymptotic range (here 13 d.o.f. per wavelength is enough for that, Sub-figure 5(d)), the pollution disappears and both upper bounds become almost identical.

It is remarkable that the new upper bounds are sharper than the classical ones just when it is needed, that is, in the pre-asymptotic regime when the number of nodes per wavelength is below 13. In the asymptotic regime, Helmholtz equation over a single element behaves like Laplace equation (since the L^2 term becomes negligible), and the corresponding upper bounds coincide, as expected.

[Figure 5 about here.]

Figure 6 shows upper bounds for the case where we consider the output functional l defined in 3.2. The observed behaviour is similar as in the previous case. Figure 6 displays the upper bounds compared to the quantity of interest, Figure 7 describes the norms of the errors, and Figures 8 and 9 show how the errors ε_h and $\widetilde{\varepsilon}_h$ are affected by the pollution effect. The same conclusions than in the previous case apply here. Additionally, we observe that the errors of the dual problems are smaller than that of the original problem (see Figure 7) because the right hand side is now localisable. Finally, Figures 8(c) and 8(d) show that the errors of the 1D Laplace equation $\widetilde{\epsilon_h}$ are null at the nodes of the mesh, as expected, which implies that the pollution error is vanishing.

[Figure 6 about here.]

[Figure 7 about here.]

[Figure 8 about here.]

[Figure 9 about here.]

5.2. Uniform h-refinements

Now, we consider the case of uniform h-refinements (see Algorithm 1). As in the previous cases, Figure 10 shows that the new bound provides a sharper estimation of the error in the quantity of interest $l(e_h)$ also when performing uniform h-refinements. Indeed, this figure exhibits the same behaviour than the p-uniform refinements case (Figure 6). The new estimate is sharper than the classical one. We also distinguish the same behaviour for the pre-asymptotic and asymptotic regimes.

[Figure 10 about here.]

Figure 11 displays the L^2-norm and H^1 semi-norm of the errors ε_h, e_h, $\widetilde{\varepsilon}_h$ and $\widetilde{e}_h$. We observe similar results as those shown in Figure 4, i.e., we have smaller errors for the tilde-version for the pre-asymptotic range and similar ones for the asymptotic range.

[Figure 11 about here.]

5.3. p-Adaptivity

We now consider Algorithm 2 with the following parameters: the wavenumber is equal to $k = 128$, the error tolerance on the quantity of interest used as stopping criteria of the algorithm is set to $tol = 10^{-4}$, and the rate of refined elements at each refinement is set to $tol_2 = 60\%$. The number of elements N is set so that the minimum number of degrees of freedom per wavelength is 3 so we satisfy the Nyquist rate, but also ensuring that we have a minimum of five

elements in total. We also have to define a refinement criterion. In Algorithm 2, we selected the simple rule:

$$\frac{|b_K(e_{h,p}, \varepsilon_{h,p})|}{\max_K |b_K(e_{h,p}, \varepsilon_{h,p})|} \cdot 100 \geqslant tol_2.$$

However, we can also consider the following alternative rule using the projected errors in the coarse mesh:

$$\frac{\left|b_K(e_{h,p}^{\text{proj}}, \varepsilon_{h,p}^{\text{proj}})\right|}{\max_K \left|b_K(e_{h,p}^{\text{proj}}, \varepsilon_{h,p}^{\text{proj}})\right|} \cdot 100 \geqslant tol_2.$$

For the new bounds, the corresponding refinement criteria become:

$$\frac{\left|\widetilde{b}_K(e_{h,p}, \widetilde{\varepsilon}_{h,p})\right|}{\max_K \left|\widetilde{b}_K(e_{h,p}, \widetilde{\varepsilon}_{h,p})\right|} \cdot 100 \geqslant tol_2 \quad \text{and} \quad \frac{\left|\widetilde{b}_K(e_{h,p}^{\text{proj}}, \widetilde{\varepsilon}_{h,p}^{\text{proj}})\right|}{\max_K \left|\widetilde{b}_K(e_{h,p}^{\text{proj}}, \widetilde{\varepsilon}_{h,p}^{\text{proj}})\right|} \cdot 100 \geqslant tol_2.$$

Figure 12 displays the upper bounds computed with and without the projections. When considering a simple p-adaptive algorithm without projections, the classical bounds provide a non-convergent algorithm (see Figure 12(a)). For this reason, projectors are introduced in order to ensure convergence (see Figure 12(b)). With the new bounds, we recover convergence even without using the projected errors, as shown in Figures 12(c) and 12(d). We believe that this behavior is strongly linked to properties of the 1D-Laplace operator. Notice that the projected error is built so that its value is null at the nodes of the mesh in order to kill the pollution effect. The 1D-Laplace operator has the same property. We expect to loose this property when using other operators for $\widetilde{b}$.

In all cases, the upper bounds behave in the same way than for the uniform refinements in the sense that the new upper bounds are sharper than the classical ones during the pre-asymptotic phase and similar for the asymptotic phase.

[Figure 12 about here.]

5.4. Modifying the alternative bilinear form

One feature of the proposed method is that we can select the alternative bilinear form $\widetilde{b}$. One could expect that the sharpness of the bounds will depend strongly on such choice. Figure 13 describes the bounds obtained when using

$$\widetilde{b}(u, v) = \langle u \, , v \rangle_{L^2(0,1)} \tag{5.3}$$

for computing the error representation compared to the bound obtained when using the Laplacian operator. We display the upper bounds both for h-uniform and p-uniform refinements. We observe that: (a) the upper bounds are sharper in the pre-asymptotic range than the classical ones, and (b) the upper bounds corresponding to the Laplace bilinear form are the sharpest in all cases.

[Figure 13 about here.]

Similarly, we now select the bilinear form

$$\widetilde{b}(u,v) = \langle \nabla u \, , \nabla v \rangle_{L^2(0,1)} + k^2 \, \langle u \, , v \rangle_{L^2(0,1)} \, . \tag{5.4}$$

Figure 14 shows the upper bounds for the case of p-uniform refinements. We obtain similar results as before and thus we draw similar conclusions, namely: (a) the new bound is better than the classical one, and (b) the bounds computed using the Laplace bilinear form are sharper. We note that the bound computed with the positive Helmholtz bilinear form (5.4) is sharper than the one computed using the L^2 scalar product (5.3), Figure 13(b).

[Figure 14 about here.]

Figure 15 illustrates how the pollution affects the errors e_h and $\widetilde{e}_h$ when considering the positive Helmholtz bilinear form (5.4). The results are similar to the case of the Laplace bilinear form. However, we now observe that error $\widetilde{e}_h$ is more affected by the pollution than in the Laplace case. Indeed, the error function is no longer null at the nodes. This may come form the fact that the 1D-Laplace equation is not affected by the pollution error. Figures 16(a) and 16(b) display the corresponding error functions for three and six points per wavelength, respectively.

[Figure 15 about here.]

[Figure 16 about here.]

6. Conclusions

This paper proposes the use of unconventional bilinear forms, different from the adjoint ones, to represent the error in the quantity of interest. Upper bounds of this error representation drive the goal oriented (or energy-norm) adaptivity process. We compared our new upper bound estimates vs those derived with the classical goal oriented methodology. We observe that our method provides sharper estimations when applied to the 1D-Helmholtz equation using the 1D-Laplacian bilinear form to represent the error. The experiments performed using different alternative bilinear forms, like the L^2-scalar product or the positive definite Helmholtz equation, show that we also obtain sharper bounds than the classical ones. Thus, we have a set of bilinear forms that may provide sharper estimates than the classical ones. This, in turn, enables us to obtain more efficient adaptive algorithms.

[1] J. Alvarez-Aramberri, D. Pardo, and H. Barucq. Inversion of magnetotelluric measurements using multigoal oriented hp-adaptivity. Procedia Computer Science, 18(0):1564 – 1573, 2013. 2013 International Conference on Computational Science.

[2] I. Babuška, F. Ihlenburg, T. Strouboulis, and S. K. Gangaraj. A posteriori error estimation for finite element solutions of Helmholtz' equation. I. The quality of local indicators and estimators. Internat. J. Numer. Methods Engrg., 40(18):3443–3462, 1997.

[3] I. Babuška, F. Ihlenburg, T. Strouboulis, and S. K. Gangaraj. A posteriori error estimation for finite element solutions of Helmholtz' equation. II. Estimation of the pollution error. Internat. J. Numer. Methods Engrg., 40(21):3883–3900, 1997.

[4] I. Babuška and W. Rheinboldt. Adaptive approaches and reliability estimations in finite element analysis. Computer Methods in Applied Mechanics and Engineering, 17:519–540, 1979.

[5] I. Babuška and W. C. Rheinboldt. A-posteriori error estimates for the finite element method. International Journal for Numerical Methods in Engineering, 12(10):1597–1615, 1978.

[6] I. M. Babuška and S. A. Sauter. Is the pollution effect of the FEM avoidable for the Helmholtz equation considering high wave numbers? SIAM Rev., 42(3):451–484 (electronic), 2000. Reprint of SIAM J. Numer. Anal. **3**4 (1997), no. 6, 2392–2423 [MR1480387 (99b:65135)].

[7] Y. Bazilevs, V. M. Calo, J. A. Cottrell, J. A. Evans, T. Hughes, S. Lipton, M. Scott, and T. Sederberg. Isogeometric analysis using T-splines. Computer Methods in Applied Mechanics and Engineering, 199(5):229–263, 2010.

[8] R. Becker and R. Rannacher. A feed-back approach to error control in finite element methods: basic analysis and examples. East-West J. Numer. Math., 4(4):237–264, 1996.

[9] R. Becker and R. Rannacher. Weighted a posteriori error control in FE methods. IWR, 1996.

[10] N. Collier, H. Radwan, L. Dalcin, and V. M. Calo. Time adaptivity in the diffusive wave approximation to the shallow water equations. Journal of Computational Science, 4(3):152–156, 2013.

[11] L. Dedè and H. Santos. B-spline goal-oriented error estimators for geometrically nonlinear rods. Computational Mechanics, 49(1):35–52, 2012.

[12] L. Demkowicz. Computing with *hp*-adaptive finite elements. Vol. 1. Chapman & Hall/CRC Applied Mathematics and Nonlinear Science Series. Chapman & Hall/CRC, Boca Raton, FL, 2007. One and two dimensional elliptic and Maxwell problems, With 1 CD-ROM (UNIX).

[13] L. E. Garcia-Castillo, D. Pardo, and L. F. Demkowicz. Energy-norm-based and goal-oriented automatic adaptivity for electromagnetics: Application to waveguide discontinuities. Microwave Theory and Techniques, IEEE Transactions on, 56(12):3039–3049, 2008.

[14] L. E. García-Castillo, D. Pardo, I. Gómez-Revuelto, and L. F. Demkowicz. A two-dimensional self-adaptive *hp* finite element method for the characterization of waveguide discontinuities. I. Energy-norm based automatic *hp*-adaptivity. Comput. Methods Appl. Mech. Engrg., 196(49-52):4823–4852, 2007.

[15] A. Günther, M. Hinze, and M. H. Tber. A posteriori error representations for elliptic optimal control problems with control and state constraints. In Constrained optimization and optimal control for partial differential equations, volume 160 of Internat. Ser. Numer. Math., pages 303–317. Birkhäuser/Springer Basel AG, Basel, 2012.

[16] M. Hintermüller and R. H. Hoppe. Goal-oriented adaptivity in pointwise state constrained optimal control of partial differential equations. SIAM Journal on Control and Optimization, 48(8):5468–5487, 2010.

[17] M. Hintermüller, R. H. Hoppe, and C. Löbhard. A dual-weighted residual approach to goal-oriented adaptivity for optimal control of elliptic variational inequalities. 2012.

[18] F. Ihlenburg and I. Babuška. Dispersion analysis and error estimation of Galerkin finite element methods for the Helmholtz equation. Internat. J. Numer. Methods Engrg., 38(22):3745–3774, 1995.

[19] F. Ihlenburg and I. Babuška. Finite element solution of the Helmholtz equation with high wave number. I. The *h*-version of the FEM. Comput. Math. Appl., 30(9):9–37, 1995.

[20] F. Ihlenburg and I. Babuška. Finite element solution of the Helmholtz equation with high wave number. II. The *h*-*p* version of the FEM. SIAM J. Numer. Anal., 34(1):315–358, 1997.

[21] C. Jhurani and L. Demkowicz. Multiscale modeling using goal-oriented adaptivity and numerical homogenization. Part I: Mathematical formulation and numerical results. Comput. Methods Appl. Mech. Engrg., 213/216:399–417, 2012.

[22] C. Jhurani and L. Demkowicz. Multiscale modeling using goal-oriented adaptivity and numerical homogenization. Part II: Algorithms for the Moore-Penrose pseudoinverse. Comput. Methods Appl. Mech. Engrg., 213/216:418–426, 2012.

[23] G. Kuru, C. V. Verhoosel, K. G. van der Zee, and E. H. van Brummelen. Goal-adaptive Isogeometric Analysis with hierarchical splines. Comput. Methods Appl. Mech. Engrg., 270:270–292, 2014.

[24] Y. Maday, A. T. Patera, and J. Peraire. A general formulation for a posteriori bounds for output functionals of partial differential equations; application to the eigenvalue problem. C. R. Acad. Sci. Paris Sér. I Math., 328(9):823–828, 1999.

[25] J. T. Oden and S. Prudhomme. Goal-oriented error estimation and adaptivity for the finite element method. Comput. Math. Appl., 41(5-6):735–756, 2001.

[26] J. S. Ovall. Asymptotically exact functional error estimators based on superconvergent gradient recovery. Numerische Mathematik, 102(3):543–558, 2006.

[27] J. Panetier, P. Ladevèze, and L. Chamoin. Strict and effective bounds in goal-oriented error estimation applied to fracture mechanics problems solved with XFEM. Internat. J. Numer. Methods Engrg., 81(6):671–700, 2010.

[28] M. Paraschivoiu and A. T. Patera. A hierarchical duality approach to bounds for the outputs of partial differential equations. Comput. Methods Appl. Mech. Engrg., 158(3-4):389–407, 1998.

[29] M. Paraschivoiu, J. Peraire, and A. T. Patera. A posteriori finite element bounds for linear-functional outputs of elliptic partial differential equations. Comput. Methods Appl. Mech. Engrg., 150(1-4):289–312, 1997. Symposium on Advances in Computational Mechanics, Vol. 2 (Austin, TX, 1997).

[30] D. Pardo. Integration of hp-adaptivity with a two grid solver: applications to electromagnetics. PhD thesis, University of Texas, Austin, 2004.

[31] D. Pardo. Multigoal-oriented adaptivity for hp-finite element methods. Procedia Computer Science, 1(1):1953–1961, 2010.

[32] D. Pardo, L. Demkowicz, C. Torres-Verdín, and M. Paszynski. Two-dimensional high-accuracy simulation of resistivity logging-while-drilling (LWD) measurements using a self-adaptive goal-oriented *hp* finite element method. SIAM J. Appl. Math., 66(6):2085–2106, 2006.

[33] D. Pardo, L. Demkowicz, C. Torres-Verdín, and M. Paszynski. A self-adaptive goal-oriented *hp* finite element method with electromagnetic applications. II. Electrodynamics. Comput. Methods Appl. Mech. Engrg., 196(37-40):3585–3597, 2007.

[34] D. Pardo, L. Demkowicz, C. Torres-Verdín, and L. Tabarovsky. A goal-oriented *hp*-adaptive finite element method with electromagnetic applications. I. Electrostatics. Internat. J. Numer. Methods Engrg., 65(8):1269–1309, 2006.

[35] D. Pardo, L. E. García-Castillo, L. F. Demkowicz, and C. Torres-Verdín. A two-dimensional self-adaptive hp finite element method for the characterization of waveguide discontinuities. part ii: Goal-oriented hp-adaptivity. Computer Methods in Applied Mechanics and Engineering, 196(49):4811–4822, 2007.

[36] J. Peraire and A. T. Patera. Bounds for linear-functional outputs of coercive partial differential equations: local indicators and adaptive refinement. In Advances in adaptive computational methods in mechanics (Cachan, 1997), volume 47 of Stud. Appl. Mech., pages 199–216. Elsevier Sci. B. V., Amsterdam, 1998.

[37] J. Peraire and A. T. Patera. Asymptotic a posteriori finite element bounds for the outputs of noncoercive problems: the Helmholtz and Burgers equations. Comput. Methods Appl. Mech. Engrg., 171(1-2):77–86, 1999.

[38] S. Prudhomme and J. T. Oden. On goal-oriented error estimation for elliptic problems: application to the control of pointwise errors. Comput. Methods Appl. Mech. Engrg., 176(1-4):313–331, 1999. New advances in computational methods (Cachan, 1997).

[39] R. Rannacher and F.-T. Suttmeier. A posteriori error control in finite element methods via duality techniques: application to perfect plasticity. Comput. Mech., 21(2):123–133, 1998.

[40] A. Romkes and J. T. Oden. Adaptive modeling of wave propagation in heterogeneous elastic solids. Comput. Methods Appl. Mech. Engrg., 193:539–559, 2004.

[41] J. Sarrate, J. Peraire, and A. Patera. A posteriori finite element error bounds for non-linear outputs of the Helmholtz equation. Internat. J. Numer. Methods Fluids, 31(1):17–36, 1999. Tenth International Conference on Finite Elements in Fluids (Tucson, AZ, 1998).

[42] P. Šolín and L. Demkowicz. Goal-oriented *hp*-adaptivity for elliptic problems. Comput. Methods Appl. Mech. Engrg., 193(6-8):449–468, 2004.

[43] L. M. Steffens and P. Díez. A simple strategy to assess the error in the numerical wave number of the finite element solution of the Helmholtz equation. Comput. Methods Appl. Mech. Engrg., 198(15-16):1389–1400, 2009.

[44] L. M. Steffens, N. Parés, and P. Díez. Estimation of the dispersion error in the numerical wave number of standard and stabilized finite element approximations of the Helmholtz equation. Internat. J. Numer. Methods Engrg., 86(10):1197–1224, 2011.

[45] K. G. van der Zee, J. T. Oden, S. Prudhomme, and A. Hawkins-Daarud. Goal-oriented error estimation for Cahn-Hilliard models of binary phase

transition. Numer. Methods Partial Differential Equations, 27(1):160–196, 2011.

[46] K. G. van der Zee, E. H. van Brummelen, I. Akkerman, and R. de Borst. Goal-oriented error estimation and adaptivity for fluid-structure interaction using exact linearized adjoints. Comput. Methods Appl. Mech. Engrg., 200(37-40):2738–2757, 2011.

[47] K. G. van der Zee and C. V. Verhoosel. Isogeometric analysis-based goal-oriented error estimation for free-boundary problems. Finite Elem. Anal. Des., 47(6):600–609, 2011.

[48] J. Waeytens, L. Chamoin, and P. Ladevèze. Guaranteed error bounds on pointwise quantities of interest for transient viscodynamics problems. Comput. Mech., 49(3):291–307, 2012.

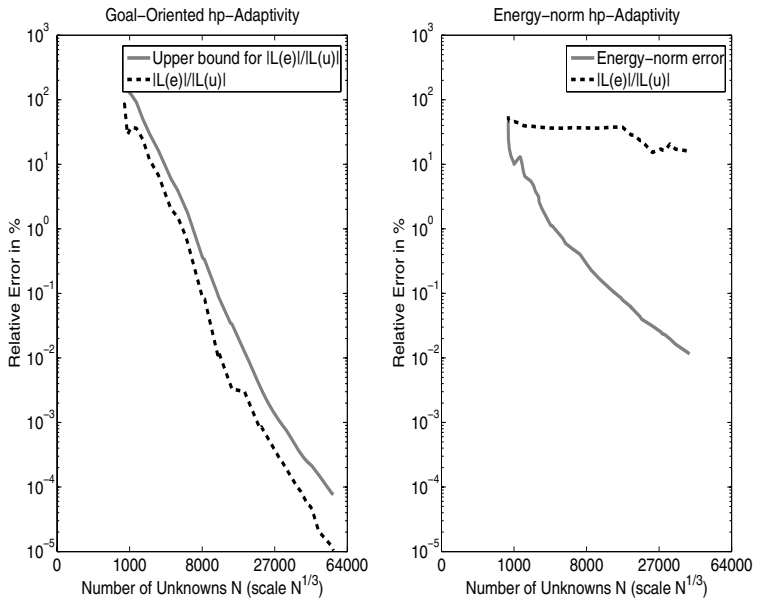

Figure 1: Left panel: convergence behaviour obtained with the self-adaptive goal-oriented hp-FEM shows exponential convergence rates. The dashed curve describes the relative error in the quantity of interest. Right panel: convergence behaviour obtained with the self-adaptive energy-norm hp-FEM shows exponential convergence rates for the energy-norm. The dashed curve describes the relative error in the quantity of interest, see [30].

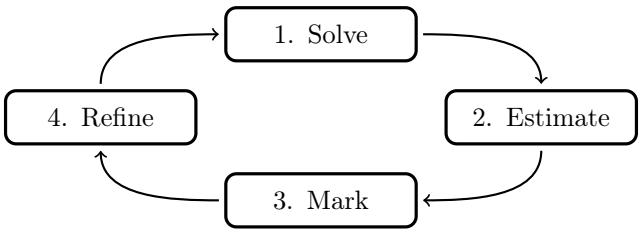

Figure 2: Classical adaptive pattern

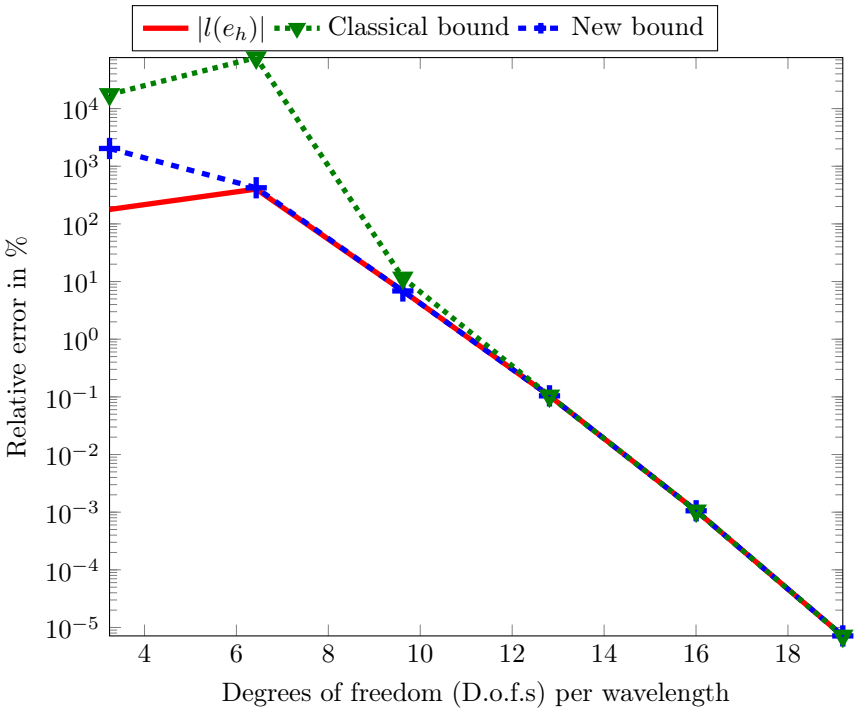

Figure 3: Upper bounds with uniform p-refinements, $l \equiv f$, $k = 128$.

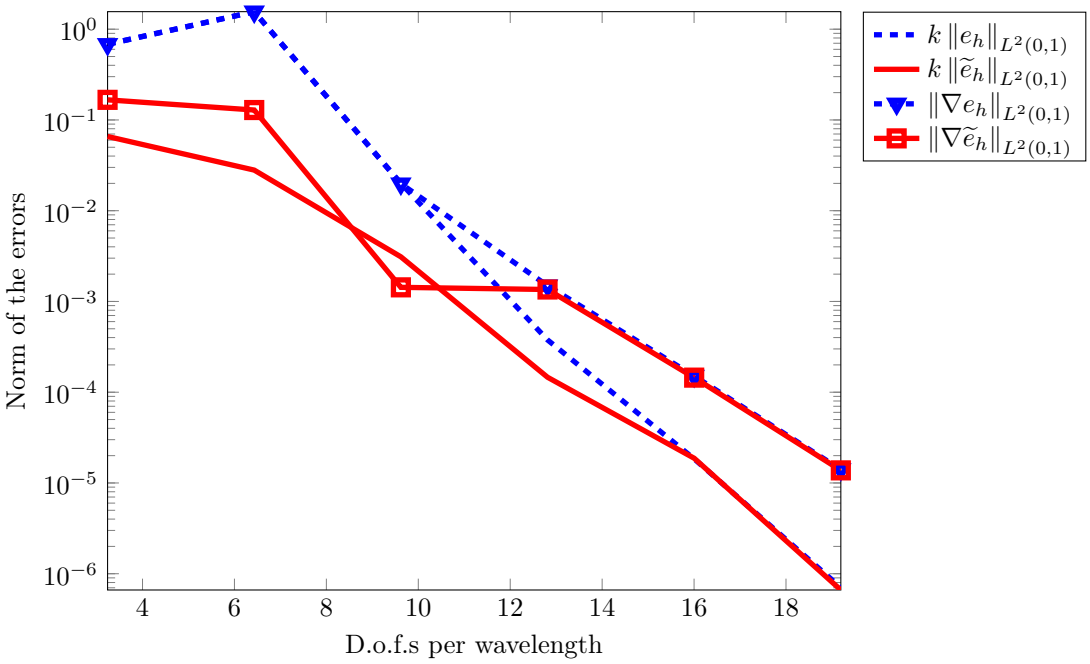

Figure 4: Norm of the errors for uniform energy-norm p-refinements, $k = 128$.

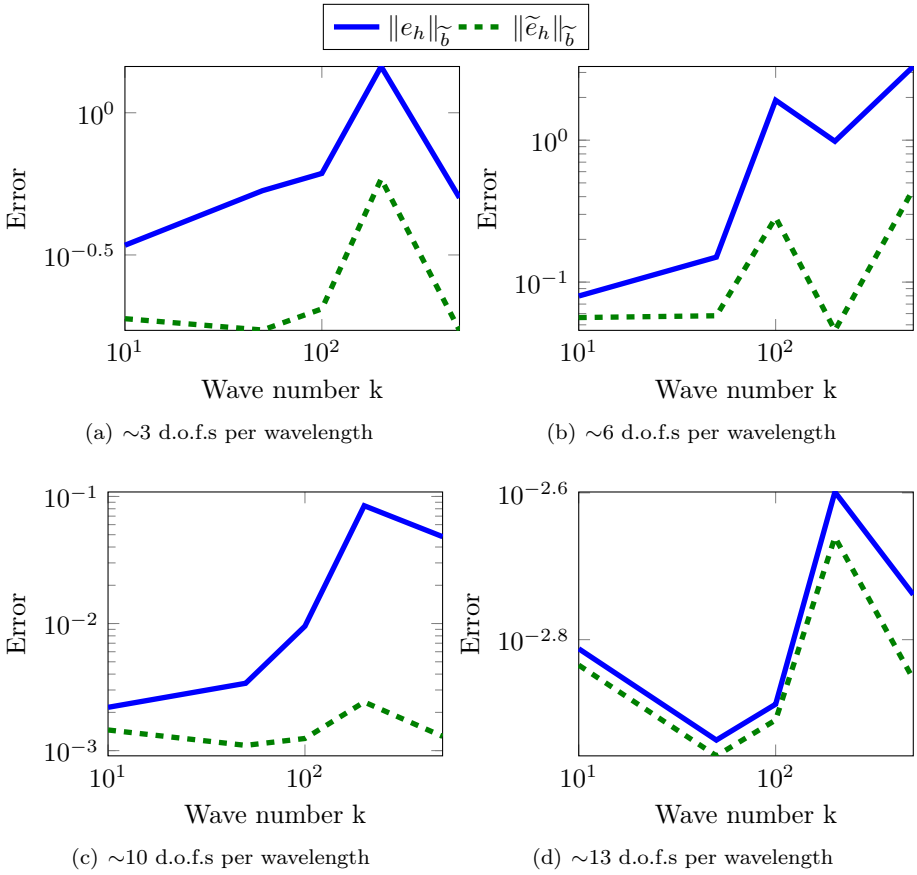

(a) ∼3 d.o.f.s per wavelength

(b) ∼6 d.o.f.s per wavelength

(c) ∼10 d.o.f.s per wavelength

(d) ∼13 d.o.f.s per wavelength

Figure 5: Norm of the errors e_h and $\widetilde{e}_h$ when increasing the wavenumber k with $\widetilde{b}$ being the Laplacian operator using uniform p-refinements.

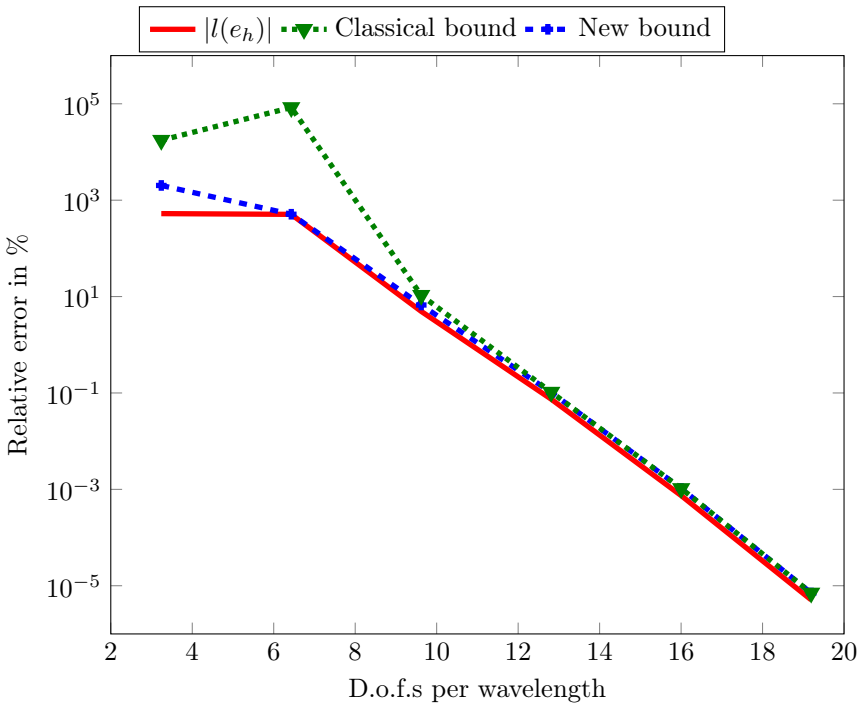

Figure 6: Bounds for uniform p-refinements for $k = 128$ and $h = 0.0154$.

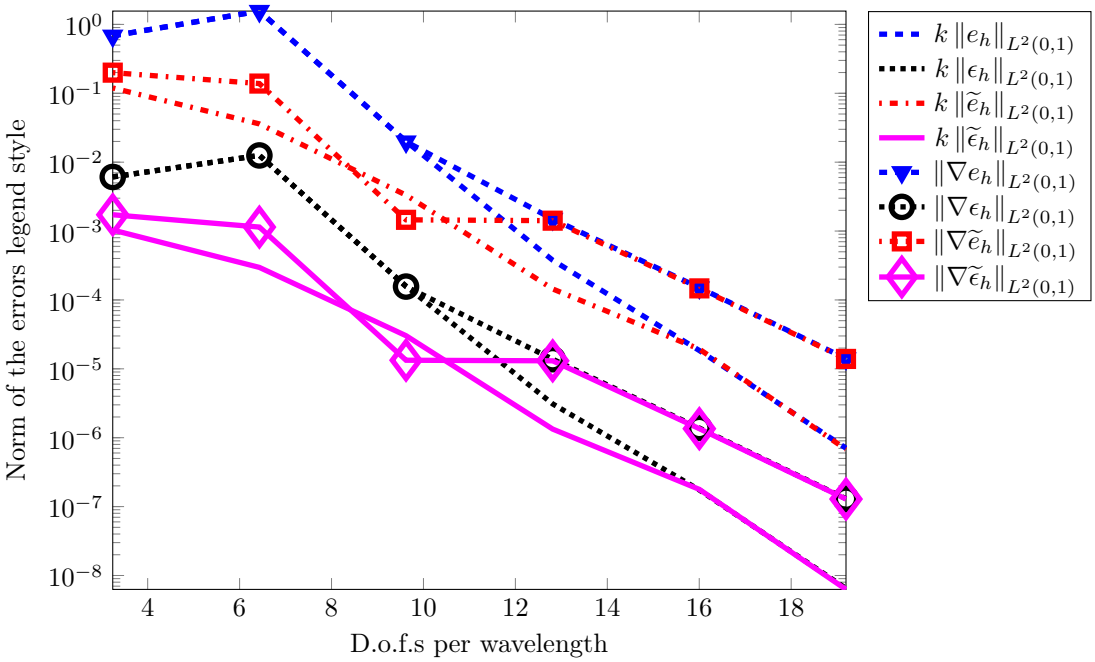

Figure 7: Norm of the errors for uniform goal oriented p-refinements, $k = 128$.

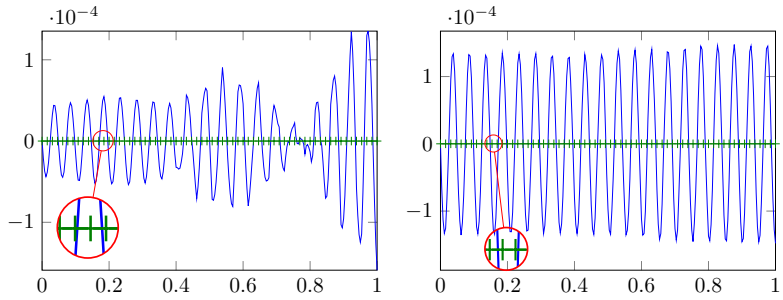

(a) ε_h with ∼3 d.o.f.s per wavelength

(b) ε_h with ∼6 d.o.f.s per wavelength

(c) $\widetilde{\varepsilon}_h$ with ∼3 d.o.f.s per wavelength

(d) $\widetilde{\varepsilon}_h$ with ∼6 d.o.f.s per wavelength

Figure 8: Error functions ε_h and $\widetilde{\varepsilon}_h$ with $\widetilde{b}$ being the Laplace operator using uniform p-refinements, $k = 128$.

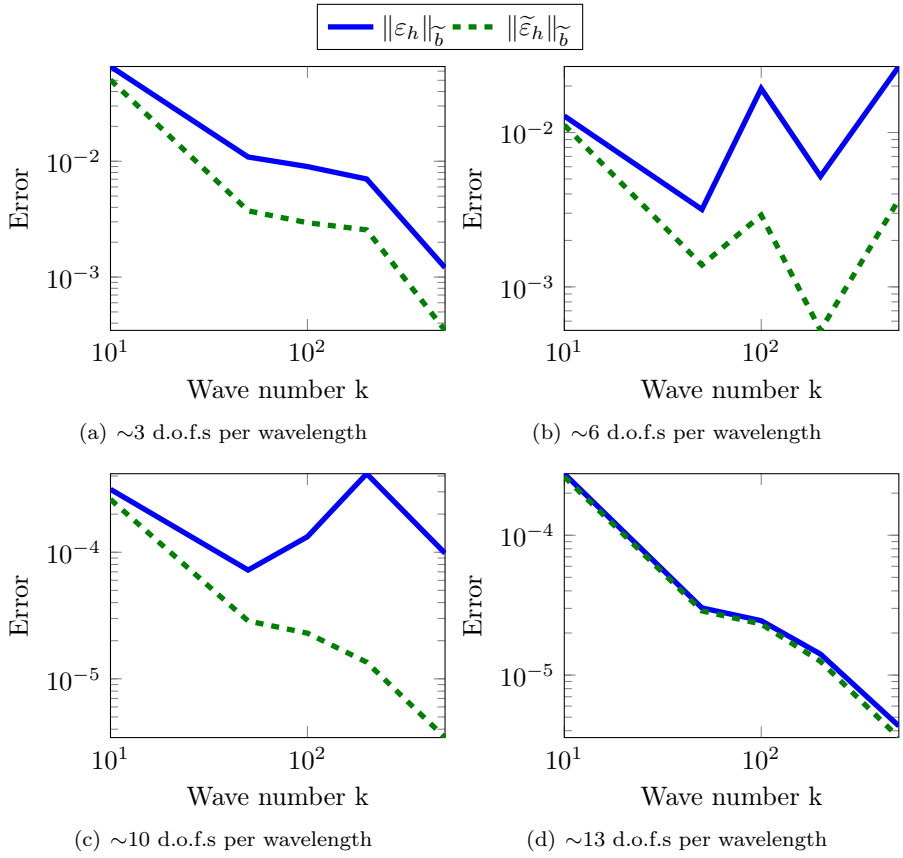

(a) ∼3 d.o.f.s per wavelength

(b) ∼6 d.o.f.s per wavelength

(c) ∼10 d.o.f.s per wavelength

(d) ∼13 d.o.f.s per wavelength

Figure 9: Norm of the errors ε_h and $\widetilde{\varepsilon}_h$ when increasing the wavenumber k with $\widetilde{b}$ being the Laplace operator using uniform p-refinements.

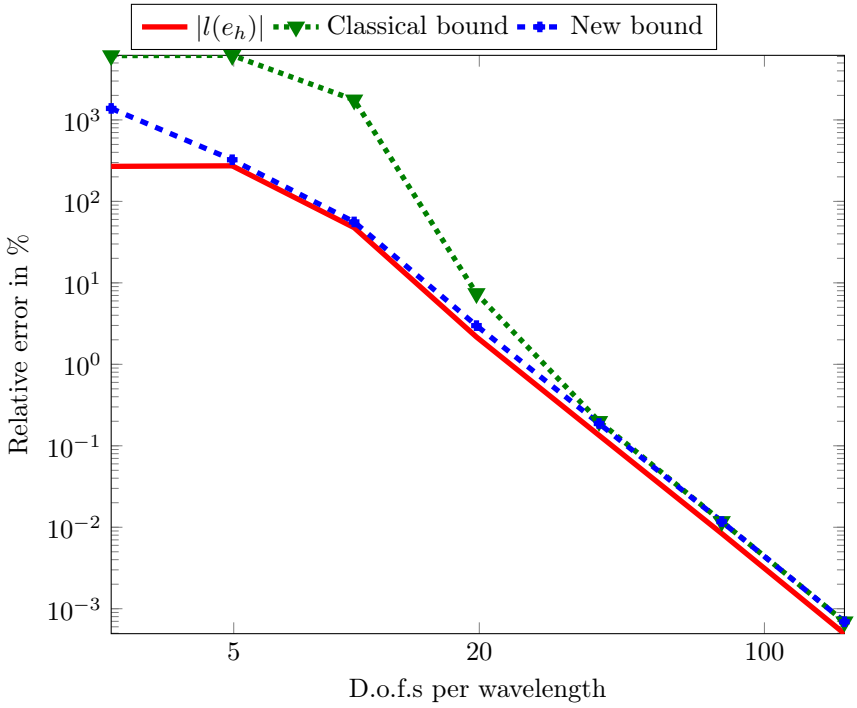

Figure 10: Upper bounds for uniform h-refinements for $k = 128$ and $p = 2$.

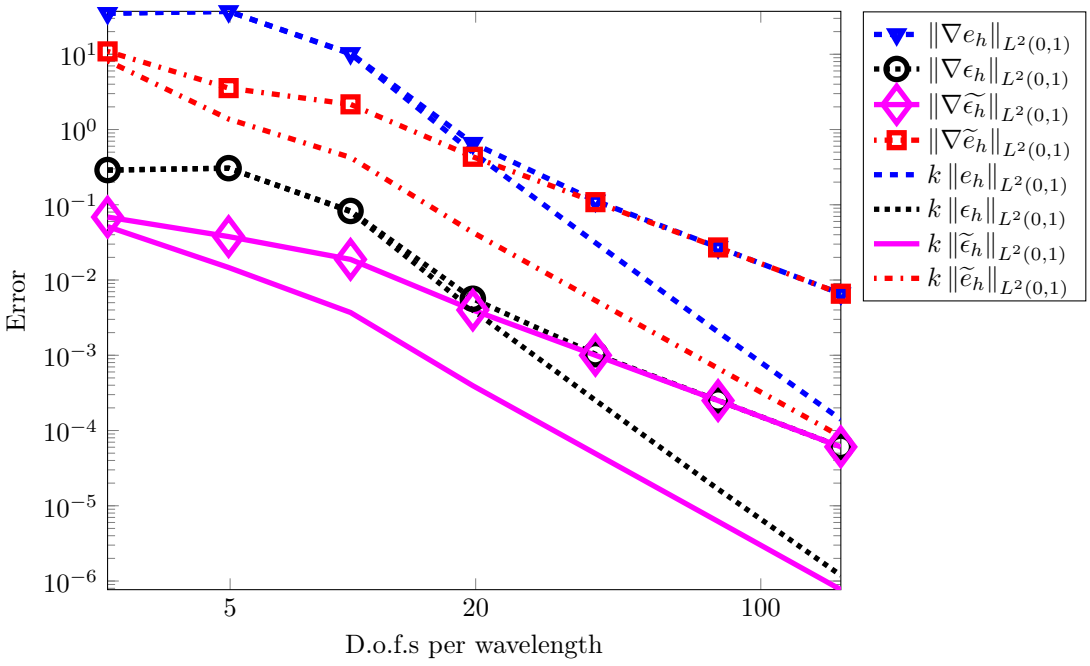

Figure 11: Norms of the errors for uniform h-refinements for $k = 128$ and $p = 2$.

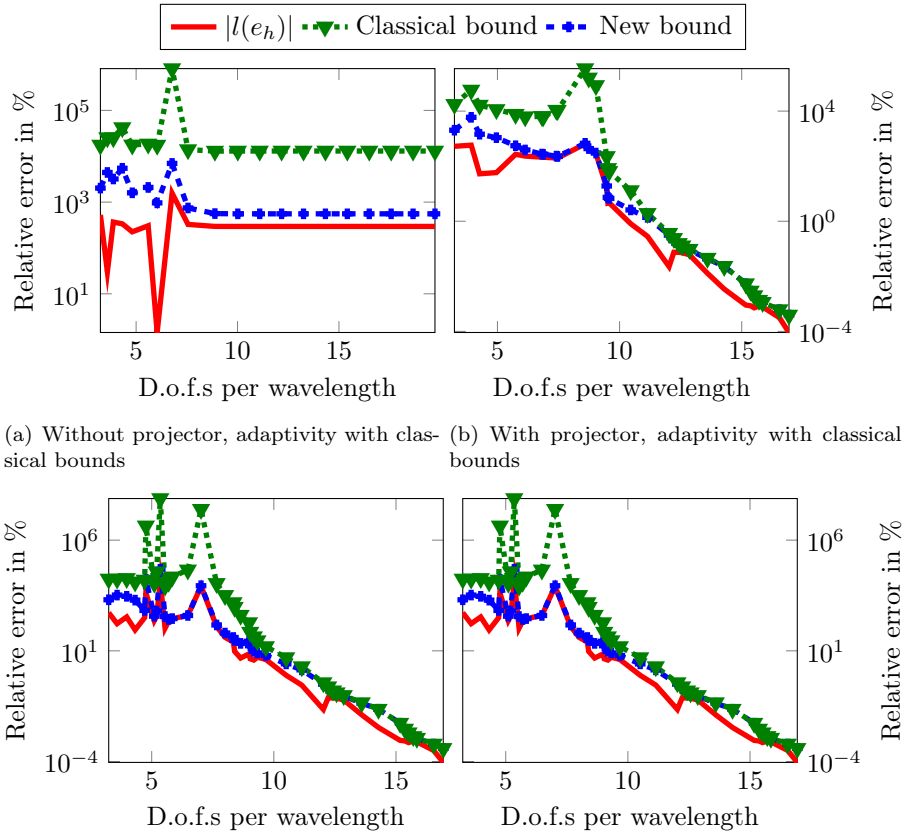

(a) Without projector, adaptivity with classical bounds

(b) With projector, adaptivity with classical bounds

(c) Without projector, adaptivity with new bounds

(d) With projector, adaptivity with new bounds

Figure 12: Bounds for p-refinements for $k = 128$ and $h = 0.0154$.

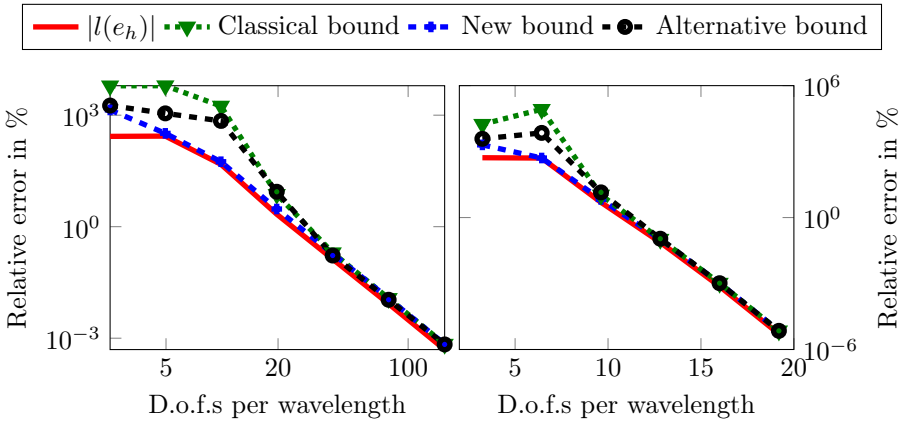

(a) uniform h-refinements (b) uniform p-refinements

Figure 13: Alternative upper bounds for uniform $h-$ and $p-$refinements using $\widetilde{b}(u,v) = \langle u\,,v\rangle_{L^2(0,1)}$, $k = 128$.

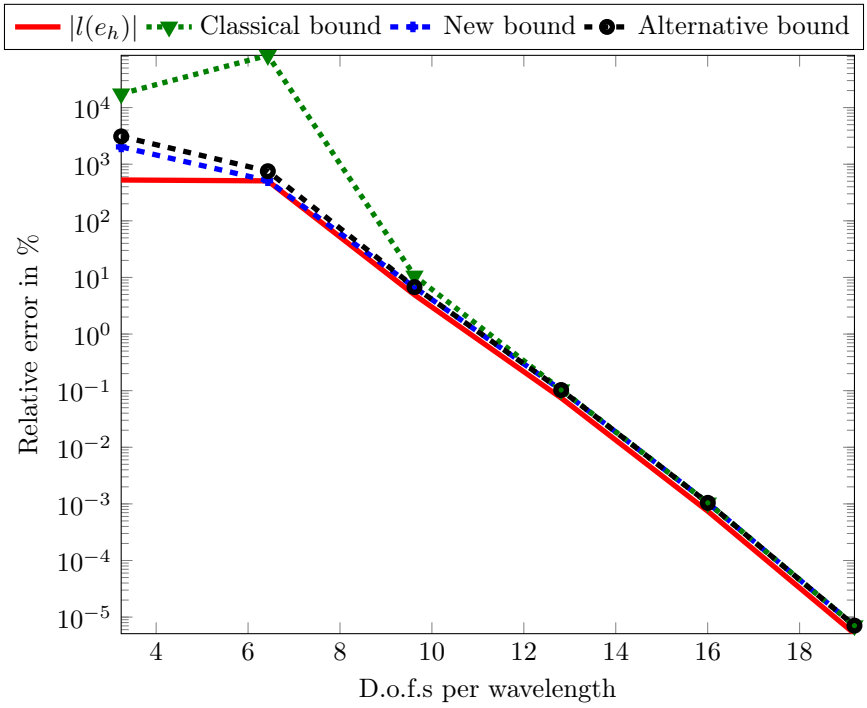

Figure 14: Alternative upper bounds for uniform $p-$refinements using $\widetilde{b}(u,v) = \langle \nabla u \, , \nabla v \rangle_{L^2(0,1)} + k^2 \, \langle u \, , v \rangle_{L^2(0,1)}$, $k = 128$.

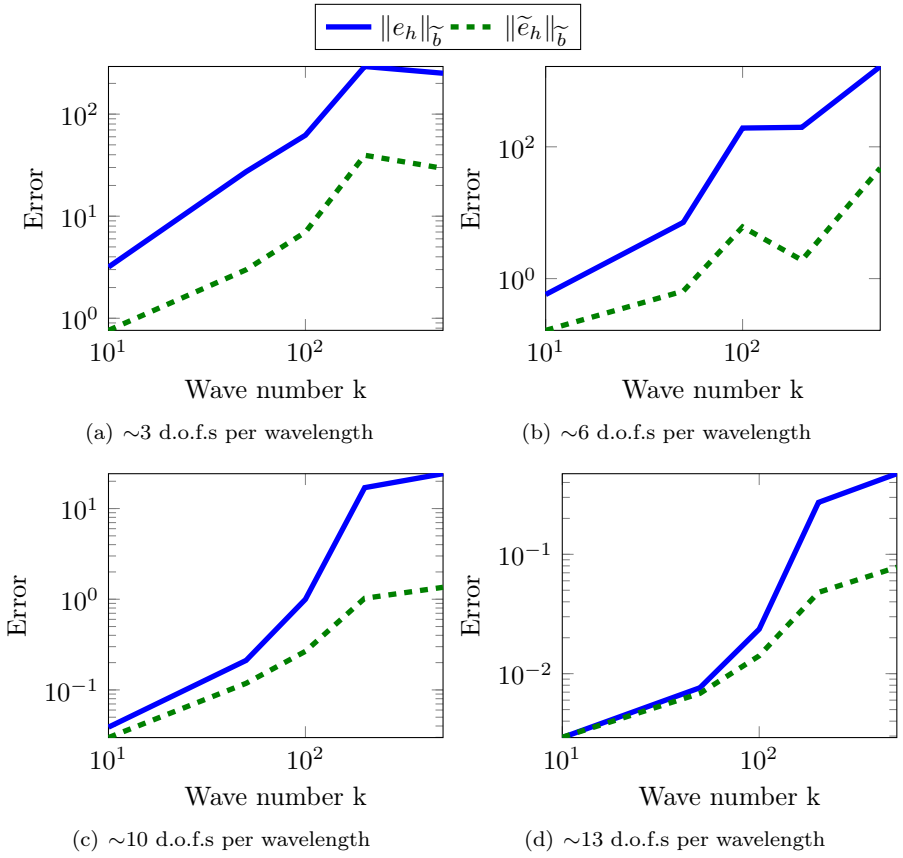

(a) ∼3 d.o.f.s per wavelength

(b) ∼6 d.o.f.s per wavelength

(c) ∼10 d.o.f.s per wavelength

(d) ∼13 d.o.f.s per wavelength

Figure 15: Norm of the errors when increasing the wavenumber k with $\widetilde{b}$ being the positive Helmholtz operator using uniform p-refinements.

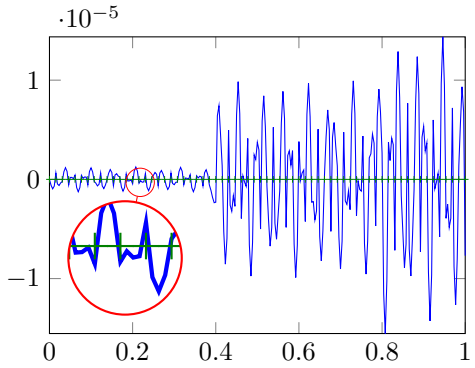

(a) $\widetilde{\varepsilon}_h$ with ∼3 d.o.f.s per wavelength

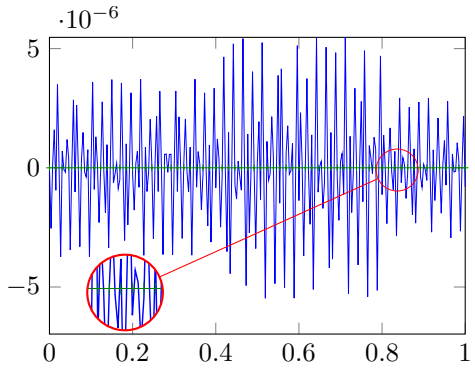

(b) $\widetilde{\varepsilon}_h$ with ∼6 d.o.f.s per wavelength

Figure 16: Error function $\widetilde{\varepsilon}_h$ with $\widetilde{b}$ being the positive Helmholtz operator using uniform p-refinements, $k = 128$.

Algorithm 1: Uniform h-refinements

Input: $N = 25$, $p = 2$

$k_{wave} = \lfloor \frac{2*\pi}{2.5} \cdot (p * N + 1) \rfloor$,

for $i \in \{1, \cdots, 10\}$ **do**

- $h_i = \frac{1}{N \cdot 2^i}$
- $u_{h_i}, v_{h_i} = \text{solve}(h_i, p, k_{wave})$ `// Solve the direct and adjoint problems`

$u_{ref} \longleftarrow u_{h_{10}}$

$v_{ref} \longleftarrow v_{h_{10}}$

for $i \in \{1, \cdots, 9\}$ **do**

- $\mathfrak{I}_{h_i}$`// compute mesh injections over the finest mesh`
- $\widetilde{\varepsilon}_{h_i} = \text{twisted\_dual}(h_{10}, p, k_{wave}, \mathfrak{I}_{h_i} v_{h_i})$ `// Solve the unconventional dual problem`
- $e_{h_i} = u_{ref} - \mathfrak{I}_{h_i} u_{h_i}$`// Estimate the errors`
- $\varepsilon_{h_i} = v_{ref} - \mathfrak{I}_{h_i} v_{h_i}$

Algorithm 2: p-adaptivity

Input: $k_{wave} = 128$, $tol = 0.001\%$, $tol_2 = 60\%$
$N = \lfloor \frac{3*k_{wave}}{2\pi} \cdot \frac{1}{5} \rfloor \cdot 5$, $h = \frac{1}{N}$

We define the mesh $\mathcal{T}_{h,p} = \cup_{i=1}^{N} K_i$ where $p = [p_1, \cdots, p_N]$ and p_i is the order of the polynomial basis in the element K_i

`// Initialisation for the adaptivity:`

$p = [1, \cdots, 1]$

while relative_error$\geqslant tol$ & $\max(p) \leqslant 15$ **do**

- $j \longleftarrow j + 1$
- `// Solve the direct and adjoint problems`
- $u_{h,p}, v_{h,p} = \text{solve}(h, p, k_{wave})$
- `// Find the reference solution of the direct and adjoint problems`
- $u_{h,p}^{ref}, v_{h,p}^{ref} = \text{solve}(h, p+2, k_{wave})$
- `// Compute the mesh injection`
- $\mathfrak{I}_{h,p}$
- `// Compute the Projection Based Interporlants as described in [12]`
- $\Pi_{h,p}(u_{h,p}^{ref})$, $\Pi_{h,p}(v_{h,p}^{ref})$
- `// Resolution of the unconventional dual problems`
- $\widetilde{\varepsilon}_{h,p}, \widetilde{e}_{h,p} = \text{twisted\_dual}(h, p, k_{wave}, \mathfrak{I}_{h,p} u_{h,p}, \mathfrak{I}_{h,p} v_{h,p})$
- $\widetilde{\varepsilon}_{h,p}^{\text{proj}}, \widetilde{e}_{h,p}^{\text{proj}} = \text{twisted\_dual}(h, p, k_{wave}, \mathfrak{I}_{h,p}\Pi_{h,p}(u_{h,p}^{ref}), \mathfrak{I}_{h,p}\Pi_{h,p}(v_{h,p}^{ref}))$
- `// Estimation of the interpolated errors`
- $e_{h,p}^{\text{proj}} = u_{h,p}^{ref} - \mathfrak{I}_{h,p}\Pi_{h,p}(u_{h,p}^{ref})$
- $\varepsilon_{h,p}^{\text{proj}} = v_{h,p}^{ref} - \mathfrak{I}_{h,p}\Pi_{h,p}(v_{h,p}^{ref})$
- `// Estimation of the actual errors`
- $e_{h,p} = u_{h,p}^{ref} - \mathfrak{I}_{h,p} u_{h,p}$
- $\varepsilon_{h,p} = v_{h,p}^{ref} - \mathfrak{I}_{h,p} v_{h,p}$
- $\text{relative\_error} = \dfrac{|l(e_{h,p})|}{\left|l(u_{h,p}^{ref})\right|} \cdot 100$
- **if** relative_error$\geqslant tol$ **then**
  - `// Execute refinements`
  - **foreach** $i \in \{1, \cdots, N\}$ **do**
    - $\text{test\_refinement} = \dfrac{|b_{K_i}(e_{h,p}, \varepsilon_{h,p})|}{\max\limits_i |b_{K_i}(e_{h,p}, \varepsilon_{h,p})|} \cdot 100$
    - **if** test_refinement$\geqslant tol_2$ **then**
      - $p_i \longleftarrow p_i + 1$
    - **else**
      - $p_i \longleftarrow p_i$